Heterozygous *PNPT1* Variants Cause Spinocerebellar Ataxia Type 25

Mathieu Barbier, PhD [1†] Melanie Bahlo, PhD [2,3†] Alessandra Pennisi, MD [4,5]
Maxime Jacoupy, PhD [1] Rick M. Tankard, PhD [2,3] Claire Ewenczyk, MD, PhD, [1]
Kayli C. Davies, BSc, [6,7] Patricia Lino-Coulon, MSc [1] Claire Colace, BSc [1]
Haloom Rafehi, PhD [2,3] Nicolas Auger, BSc, [1,8] Brendan R. E. Ansell, MD [2,3]
Ivo van der Stelt, BSc, [2,3,9] Katherine B. Howell, MD, PhD [7,10,11]
Marie Coutelier, MD, PhD, [1,8] David J. Amor, MD, PhD [7,11] Emeline Mundwiller, MSc, [1]
Lena Guillot-Noël, MSc, [1,8] Elsdon Storey, MD, PhD, [12] R. J. McKinlay Gardner, MD, [13]
Mathew J. Wallis, MD [14,15] Alfredo Brusco, PhD [16] Olga Corti, PhD [1]
Agnès Rötig, PhD [4,5] Richard J. Leventer, MD, PhD [7,10,11] Alexis Brice, MD [1]
Martin B. Delatycki, MD, PhD, [6,7,17] Giovanni Stevanin, PhD [1,8‡]
Paul J. Lockhart, PhD [6,7‡] and Alexandra Durr, MD, PhD [1‡]

Objective: Dominant spinocerebellar ataxias (SCA) are characterized by genetic heterogeneity. Some mapped and named *loci* remain without a causal gene identified. Here we applied next generation sequencing (NGS) to uncover the genetic etiology of the *SCA25 locus*.
Methods: Whole-exome and whole-genome sequencing were performed in families linked to *SCA25*, including the French family in which the *SCA25 locus* was originally mapped. Whole exome sequence data were interrogated in a cohort of 796 ataxia patients of unknown etiology.
Results: The SCA25 phenotype spans a slowly evolving sensory and cerebellar ataxia, in most cases attributed to ganglionopathy. A pathogenic variant causing exon skipping was identified in the gene encoding Polyribonucleotide Nucleotidyltransferase PNPase 1 (*PNPT1)* located in the *SCA25* linkage interval. A second splice variant in *PNPT1* was detected in a large Australian family with a dominant ataxia also mapping to *SCA25*. An additional nonsense variant was detected in an unrelated individual with ataxia. Both nonsense and splice heterozygous variants result in premature stop codons, all located in the S1-domain of PNPase. In addition, an elevated type I interferon response was observed in blood from all affected heterozygous carriers tested. PNPase notably prevents the abnormal accumulation of

View this article online at wileyonlinelibrary.com. DOI: 10.1002/ana.26366

Received Nov 7, 2021, and in revised form Apr 4, 2022. Accepted for publication Apr 8, 2022.

Address correspondence to Prof Durr, Paris Brain Institute, Hopital Pitié-Salpêtrière, 47, boulevard de l'Hôpital CS21414, 75,646 PARIS CEDEX 13. E-mail: alexandra.durr@icm-institute.org; and Prof Lockhart, Bruce Lefroy Centre, Murdoch Children's Research Institute, Melbourne, VI 3052. E-mail: paul.lockhart@mcri.edu.au

[†]These authors contributed equally.

[‡]Joint senior authors.

From the [1]Sorbonne Université, Institut du Cerveau—Paris Brain Institute—ICM, Inserm, CNRS, APHP, Hôpital de la Pitié Salpêtrière, Paris, France; [2]Population Health and Immunity Division, The Walter and Eliza Hall Institute of Medical Research, Melbourne, Victoria, Australia; [3]Department of Medical Biology, University of Melbourne, Melbourne, Victoria, Australia; [4]Necker Hospital, APHP, Reference Center for Mitochondrial Diseases, Genetics Department, Institut Imagine, University of Paris, Paris, France; [5]Inserm UMR_S1163, Institut Imagine, Paris, France; [6]Bruce Lefroy Centre, Murdoch Children's Research Institute, Melbourne, Victoria, Australia; [7]Department of Paediatrics, University of Melbourne, Melbourne, Victoria, Australia; [8]Paris Sciences Lettres Research University, EPHE, Paris, France; [9]Donders Centre for Neuroscience, Faculty of Science, Radboud University, Nijmegen, The Netherlands; [10]Department of Neurology, Royal Children's Hospital, Melbourne, Victoria, Australia; [11]Murdoch Children's Research Institute, Melbourne, Victoria, Australia; [12]School of Public Health and Preventive Medicine, Monash University, Melbourne, Victoria, Australia; [13]Clinical Genetics Group, University of Otago, Dunedin, New Zealand; [14]Clinical Genetics Service, Austin Health, Melbourne, Australia; Department of Medicine, University of Melbourne, Austin Health, Melbourne, Australia; [15]School of Medicine and Menzies Institute for Medical Research, University of Tasmania, Hobart, Tasmania, Australia; [16]Department of Medical Sciences, University of Torino, Torino, Italy; and [17]Victorian Clinical Genetics Service, Melbourne, Australia

double-stranded mtRNAs in the mitochondria and leakage into the cytoplasm, associated with triggering a type I interferon response.
Interpretation: This study identifies *PNPT1* as a new SCA gene, responsible for SCA25, and highlights biological links between alterations of mtRNA trafficking, interferonopathies and ataxia.

ANN NEUROL 2022;92:122–137

Spinocerebellar ataxias (SCAs) are a heterogeneous group of autosomal dominant neurodegenerative disorders. Clinical presentations include cerebellar ataxia manifesting as gait disturbance, incoordination of upper limb movements, nystagmus, and dysarthria, with additional pyramidal or extrapyramidal features. A non-exhaustive list of other symptoms can be associated with SCA including peripheral neuropathy, cognitive impairment, dystonia, parkinsonism and hearing loss. Variable age at onset of symptoms is observed between and within SCA subtypes. Genetic heterogeneity is also a hallmark of SCA with 48 SCA *loci* described to date. We previously mapped the *SCA25 locus* (MIM: 608703) in a French family (family 360) in which cerebellar ataxia and prominent sensory neuropathy segregated as an autosomal dominant trait.[1] Both age of onset and severity of disease were highly variable between affected family members. Two relatives with the *SCA25* haplotype were, respectively, unaffected or very mildly affected, showing either incomplete penetrance or very late onset. At that time, the size of the region of interest and the high number of genes located in the chromosomal interval precluded identification of the causal variant.

In this study next generation sequencing (NGS) methods (whole-exome and whole-genome) were applied to uncover the genetic etiology of the *SCA25 locus*. In parallel, linkage and NGS approaches led to identify a common candidate gene, *PNPT1*, in a large Australian family with a dominant ataxia segregating also mapping for the *SCA25 locus*.

Patients and Methods

Individuals from French family SAL-360

Identification of the *SCA25 locus* was in the SAL-360 family.[1] Since then, relatives from this family were seen by A.D. at their home, and the index case was seen for follow-up in the clinic at the genetic department at the Pitié Salpêtrière Hospital in Paris. The pedigree of SAL-360 is presented in Figure 1A. Clinical presentations of affected individuals has been extensively described.[1]

Blood samples were taken after informed consent from 22 subjects, including 6 clinically affected subjects: III-14, III-32, IV-23 IV-24, IV-28 (proband), and IV-40; 1 very mildly affected (III-18); 12 unaffected at-risk subjects: III-13, III-17, III-43, III-44, III-33, III-20, III-21, III-22, IV-35, IV-36, IV-27; and IV-29 and 3 spouses (II-8, III-15, and III-19). Skin biopsies were performed on two brothers IV-27 (healthy at-risk) and IV-28 (affected).

A cohort of 796 French individuals with ataxia, recruited via the Spatax network (https://spatax.wordpress.com/), who had whole exome sequencing (WES) and who did not have a causal pathogenic variant identified previously were analyzed for *PNPT1* variants.

Individuals from the Australian A1 family

Blood was collected from 10 individuals (Fig 1B; II-1, II-3, III-1, III-2, III-4, III-5, III-6, IV-1, IV-2, IV-3) and genomic DNA was extracted using the BACC DNA extraction kit (GE Healthcare Life Sciences, Uppsala, Sweden), according to the manufacturer's protocols. Detailed clinical neurological assessments, brain MRI scanning and nerve conduction studies are presented in Tables 1–3.

Ethics Committee Approval

The study was conducted in line with the Declaration of Helsinki and was approved by the Ethics Review Board (Paris Necker ethics committee approval (RBM 01–29 and RBM 03–48) to A.B. and A.D). Informed consent was obtained from all participants and/or their parents.

The study was also approved by the Royal Children's Hospital Human Research Ethics Committee (Approval number 28097). Informed consent was obtained from all participants and/or their parents.

Whole Exome and Whole Genome Sequencing

Family 360. WES was first performed in five individuals at IntegraGen S.A (OncoDNA group). Four affected individuals (IV-24, III-14, IV-28 and IV-40) and one spouse (III-15, father of IV-24) were selected for sequencing (Fig 1A). Genomic DNA was captured using Agilent in-solution enrichment methodology (SureSelect Human All Exon Kits Version 5, Agilent) with their biotinylated oligonucleotides probe library (Human All Exon v5–50 Mb, Agilent), followed by paired-end 75 bases massively parallel sequencing on Illumina HiSEQ 2000. The bio-infomatics analysis of sequencing data was based on the Illumina pipeline (CASAVA1.8.2). Variant annotation was performed through an IntegraGen in-house pipeline. Sequencing results were filtered for a depth ≥10× and for

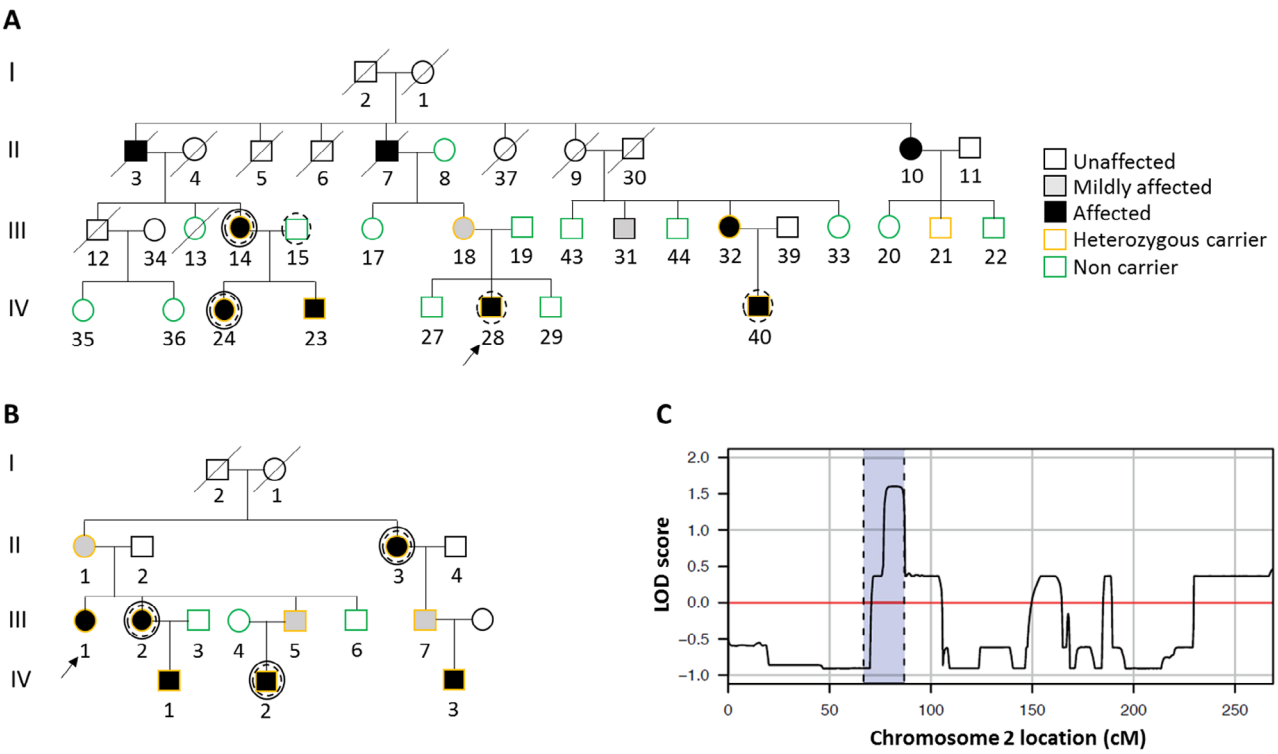

FIGURE 1: Pedigrees of families with autosomal dominant spinocerebellar ataxia mapping to the *SCA25 locus*. (A) Pedigree of the French family (360). (B) Pedigree of the A1 Australian family. Orange symbols indicate family members heterozygous for mutations in *PNPT1*. Black arrows indicate probands. DNA from circled individuals was used for whole-exome sequencing (dotted lines) or whole-genome sequencing (solid lines). (C) Multipoint LOD scores from parametric linkage analyses performed in the A1 family across the chromosome 2. The blue area corresponds to the *SCA25 locus* mapped previously in the French family 360.

heterozygous variants shared between these four affected relatives and not present in the unaffected father of one of them. Only variants with a minor allele frequency <0.01% in public variant databases and absent from an in-house Integragen whole-exome data set of 176 additional exomes were retained. Nonsense, missense, insertion/deletion, and splice variants were selected before applying selection filters.

Whole genome sequencing (WGS) was performed in the mother-daughter pair III-14 and IV-24 from family 360 by the deCODE Genetics Company. Briefly, Illumina's HiSeqX platform was used by generating sequencing libraries using the so-called PCR-free sample preparation method. Mean depth was at least 30x.

The candidate variant in polyribonucleotide nucleotidyltransferase 1, mitochondrial (*PNPT1*; NM_033109.5: c.2069 + 3T>C) was validated by Sanger sequencing.

Australian A1 Family

WES of individuals II-3, III-2, and IV-2 (Fig 1B) was performed at the Australian Genome Research Facility (AGRF), Melbourne, Australia. Exonic regions were enriched with the Agilent SureSelect XT Human All Exon v4 as well as v5 + untranslated region (UTR). Paired-end 100 bp sequencing was performed on an Illumina HiSeq 2,500 with target depths of 70 and 50 for the capture v4 and v5 + UTR platforms, respectively.

WGS was performed on individual IV-2 at AGRF Melbourne on four lanes of an Illumina HiSeq 2,500 in rapid-run mode, producing 150 bp paired-end reads with a target depth of 48x. WGS was also performed for II-3 and III-2 on the Illumina HiSeq X Ten producing 151 bp paired-end reads with target depth of 60x at the Kinghorn Centre for Clinical Genomics, Darlinghurst, Australia. FastQ data was aligned with Bowtie2 (version 2.2.5) and reads were sorted and merged by Novosort v1.03.07. Variant calling was performed with the HaplotypeCaller in GATK. Variants were filtered that did not fit the following criteria: within 1 Mb of the linkage regions (as given by the SNP chip linkage analysis below), alternative allele frequency equal to or less than 0.01 in the 1,000 Genomes Project[2] (ANNOVAR 1000g2012feb), NHLBI 6500 exomes and ExAC (release 0.3) databases, less than 10 observed alleles in 132 in-house control samples, in an ORF or within 5 bp of a splice site, and not a synonymous change. As the three samples sequenced were all from affected individuals we expected heterozygous calls under the dominant disease model. Candidate variants underwent validation by standard Sanger sequencing.

SNP Chip Linkage Analysis

All available DNA samples from the Australian family were hybridized to the Illumina HumanCytoSNP-12 v2.1 SNP chip. SNP genotypes were called in Illumina BeadStudio. Relatedness was verified with XIBD[3] (Supplementary Materials and Methods, which are available online). Inbreeding coefficients were estimated with FEstim[4] and LINKDATAGEN[5] selected 11,995 SNP markers for linkage analysis performed essentially as described previously.[6]

The obligate carrier II-1 was modeled as unknown. As SCAs may be a late-onset disorder, the two unaffected samples with data were modelled with unknown affectedness status.

Copy-Number Variant Analysis

Copy-number variants (CNVs) were detected with the SNP chip data using PennCNV[7] independently for each sample in the Australian family A1. CNVs were also called using the WGS data of individuals II-3 and III-2 and 15 in-house controls whose data were generated at the same sequencing center.

Repeat Expansion Analysis

In the French family 360, WGS data from affected individuals III-14 and IV-24 was analyzed with Expansion hunter (v.3.0)[8] to exclude known repeat expansion loci. BAM files were also visually inspected with the Integrative Genome Viewer (IGV) software to check for unexpected variation in read depths and to detect possible new pathogenic expansions in the *SCA25 locus*.

In the Australian family, a search for putative repeat expansions in the linkage interval was performed using ExpansionHunter Denovo.[9] STR loci with a *p*-value of less than 0.1 were further characterized using Expansion Hunter (v.3.2.0, with inclusion of off-target reads, read depth of 30, and minimum anchor-read mapping quality score of 20) and exSTRa[10] (default parameters).

RNA and Protein Analyses in the Australian Family

Lymphoblast cell lines were established for IV-2 and three unrelated control individuals. Total RNA was isolated (RNeasy, Qiagen) and libraries prepared using the TruSeq RNA V2 kit (Illumina) and sequenced to a depth of ~90 million reads. Paired end fastq files were aligned to the ENSEMBL human genome (Homo_sapiens.GRCh38.99) using STAR[11] (version 2.7.3a). Bam files were generated using samtools[12] (1.9). Read counts per gene were generated using featureCounts,[13] with a quality score cutoff of 10. Differential gene expression of IV-2 compared to the controls was determined using limma and edgeR, as described in Law et al.[14]

Western blot analysis was performed as previously described.[15] Primary antibodies (rabbit anti-PNPase (Abcam, ab96176, 1:500) and mouse anti-β-Actin (Sigma, A5441, 1:10,000) were used and images were captured with ImageQuant AI680 and quantified using ImageQuantTL software (GE Healthcare). To quantify PNPase steady state levels, individual sample values were first determined by normalizing the intensity of PNPase to the loading control β-Actin and then to the control samples, statistical significance was tested with two-tailed Student's *t* test and $p < 0.05$ was considered significant.

PNPT1 Transcripts Analysis and Proteins Immunoblots in Family 360

Primary skin fibroblasts from two brothers belonging to family 360, one affected (IV-28) carrying the variant and the other non-carrier and unaffected (IV-27), plus patient 461–7, were generated from skin biopsies. The ages at sampling were very close (48, 47, and 45 years respectively), and the number of passages was equal for all (n = 5).

Cells were cultured in DMEM—High Glucose—GlutaMAX medium supplemented with 10% fetal bovine serum (FBS) and 1% penicillin/streptomycin (Gibco). mRNA and protein were harvested from different cell pellets from prima ry skin fibroblasts grown with or without emetine to block the nonsense-mediated decay (NMD) RNA surveillance pathway.

mRNA was extracted from cell pellets with TRIzol reagent (Life Technologies) according to the manufacturer's instructions., and treated with DNase (TURBO DNA-free, Invitrogen). Reverse transcription (RT) was achieved with the SuperScript First-Strand Synthesis System kit using Oligo(dT) (Invitrogen). Primers were designed to detect abnormal splicing between exons close to the variants, or to detect intron-retention. RT-PCR products were then sequenced by standard Sanger sequencing.

Proteins were extracted after lysis of cells. Immunoblot analysis was performed with proteins from the individuals' cells using antibodies directed against N-terminal parts of PNPase (sc-365,049 from Santa Cruz Biotechnology) and rabbit anti-Alpha-Tubulin (Ab18251). Proteins were visualized with fluorescent antibodies or by enhanced chemiluminescence (Pierce) and fluorescence/chemiluminescence signals were captured with the Odyssey Imaging System (Li-COR), or with the Chemidoc Touch Imaging System (Bio-Rad) and quantified with Li-COR Image Studio (Li-COR) or Image Lab Software (Bio-Rad).

Mitochondrial Oxidative Phosphorylation (OXPHOS) Enzyme Activities

Primary fibroblasts from carriers 360–28 and 461–7, and from the non-carrier 360–27, were grown in DMEM low

glucose with D-galactose (4.5 g/L) when reaching about 50% confluence during 7 days (final confluence was <100%). Ages at collection were 47, 45, and 48, respectively. Cells were then prepared for OXPHOS assays by measuring the oxygen consumption in the temperature-regulated chamber of the Oxygraph-2 k (Oroboros, Innsbruck, Austria). The oxygen consumption was recorded sequentially for: respiration under basal conditions (R-Basal); Complex I (CX I); Oxidative phosphorylation involving complex I and V (OXP Cx I); Oxidative phosphorylation of complex I, V, and II (OXP CxII); measure of proton leakage (H-Leak); maximal capacity of respiration (ETS-max); and non-mitochondrial respiration (ROX). Details of media composition and steps to measure each parameter are available upon request.

Interferon Signature Analysis in Blood

A real-time qPCR analysis was performed on peripheral blood lymphocytes (PBLs) from carriers and non-carriers of *PNPT1* variants to assess interferon signaling pathway gene expression. Two samples with different age at sampling were available for the two brothers from family 360 and for individual 461–7, and one sample for the parents of 461–7. Total RNA was extracted from PBL pellets using TRIzol reagent, and treated with TURBO DNase (Invitrogen). RT-PCR and qPCR were performed as described previously.[16] The gene set included six interferon-stimulated genes (ISGs)[17]: *IFI27*, *IFI44L*, *IFIT1*, *ISG15*, *RSAD2*, and *SIGLEC1*. The relative abundance of each target transcript was normalized to the expression level of *GAPDH*. qPCR assays were performed in duplicate. The mean fold change of the six genes in carriers was calculated to create an interferon score for each individual.

Results

WES was performed in five individuals, four affected and one spouse (non-carrier) in family 360 (Fig 1A). The index case was initially seen at age 22 years; however, onset of symptoms was at 1 year. He was not able to run at age 3 years and had frequent vomiting during childhood. A clinical diagnosis of Friedreich ataxia was made at age 8 years, but no *FXN* expansion was found. He required a wheelchair for mobility from age 13 years. He was found to have a predominantly sensory neuropathy with moderate dysarthria and flexor plantar responses and was of normal intelligence.[1] Ocular movement recordings showed square waves, hypermetric saccades and gaze evoked nystagmus. Examination at age 32 years was notable for the presence of chronic cough, generalized wasting, with abolished vibration sense and decreased sensitivity to touch and pinprick distally. MRI showed severe cerebellar atrophy involving the vermis and hemispheres, as well as the bulbar region and medulla. There was no abnormality of the white matter. At age 50 years, he scored 30/40 on the Scale for the Assessment and Rating of Ataxia (SARA), stable for at least 4 years. Sensory neuropathy with cramps and pain, square wave jerks, and down beat nystagmus were noted. Deafness was evident at age 46 years. Because of the clinical similarity with CANVAS (sensory neuropathy, cerebellar ataxia and reduced visually enhanced vestibulo-ocular reflex), we tested for the pathological $(AAGGG)_n$ expansion in *RFC1*,[18,19] which was not found. Interestingly, his mother, an obligate carrier, was pauci-symptomatic at age 61 years with slight axial instability. Follow-up at age 79 years revealed that she had required hearing aids since the age of 65 years. On examination she showed head tremor and diplopia and scored 4/40 on the SARA. Clinical features are presented in Tables 1 and 2.

Analysis of the WES data identified a single heterozygous variant on chromosome 2 (chr2:g.55643155T>C, GRCh38/hg38) that satisfied the criteria of selection and transmission, and was absent from the gnomAD database v.2.1.1 or v.3 (https://gnomad.broadinstitute.org/). Notably, this variant lies in the region of significant linkage identified previously as *SCA25* on chromosome 2 in the same family.[1] This intronic substitution is located near the canonical exon 25 splice donor site of *PNPT1* (NM_033109.5:c.2069 + 3 A>G), a gene encoding Polyribonucleotide Nucleotidyltransferase PNPase 1 (PNPase). WGS was then performed in the affected mother-daughter pair who had previously undergone WES to search for non-sequenced variants that could have been missed using WES, and also to test for known expansion *loci* repeat length (Fig 1A). We did not detect pathogenic expanded repeats in any of the known *loci* responsible for repeat expansion diseases tested. After filtering, 32 ultra-rare variants, absent from population databases and predicted to be deleterious (Combined Annotation Dependent Depletion CADD phred score[20] >20), were shared between the two affected individuals. The c.2069 + 3 A>G substitution in *PNPT1* was the only variant that mapped to the *SCA25* locus.

In parallel, a combined strategy including linkage, WES, WGS, and RNA-Seq analysis was performed in a four-generation Australian family (family A1) with ataxia and sensory neuropathy in most affected individuals (Fig 1B). Six individuals presented with an autosomal-dominant progressive ataxia. Variable age at onset (ranging from 5 to 56 years of age) and presence of sensory neuropathy were noted (Table 3), as observed in the French family. Affected individuals had diminished or absent limb reflexes, diminished sensation, and nystagmus. Cerebellar atrophy was present on MRI in those with marked ataxia.

TABLE 1. Predominant Signs, Electroneuromyography, and Brain MRI Observations of Affected Individuals with *PNPT1* Variations in the French Index Cases from Family 360 (All Relatives Extensively Described in Stevanin et al[1]) and from Family 461 Index Case, and Carriers from the Australian Family A1

Patient	Age at Exam	Age at Onset	Predominant Sign (handicap/7)	Cerebellar Ataxia Score (SARA)	ENMG	Brain MRI
360–28 (index)	22	17 mo	Sensory and cerebellar ataxia (6)	Severe	SN	N/A
	32	17 mo	Sensory and cerebellar ataxia (6)	Severe	N/A	CA
	50	17 mo	Sensory and cerebellar ataxia (6)	Severe (30/40)	N/A	CA and BA, WM changes
461–7 (index)	40	23	Ataxia (6)	Moderate (24/40)	SN, mild myopathy	CA, WM changes
A1-II-3	58	21	Moderate cerebellar dysarthria, gross upper and lower limb ataxia	N/A	N/A	Cerebellar atrophy
A1-II-1	56	56	Very subtile incoordination	N/A	N/A	Normal
A1-III-1 (index)	20	10	Ambulant, with upper and lower limb ataxia	N/A	Reduced median nerve sensory potential, absent left median nerve sensory potential, borderline right tibial motor conduction velocity	CA
A1-III-2	21	20	Minimal gait ataxia, mild finger-nose ataxia, no dysarthria	N/A	N/A	CA
A1-III-5	37		None	N/A	SN	Normal
A1-III-7	33		None	N/A	Axonal sensory neuropathy with mild axonal motor neuropathy	Normal
A1-IV-1	6	5	Unable to tandem walk, positive Romberg sign	N/A	SN	CA
A1-IV-2	6	5	Required K-walker	N/A	SN	CA
A1-IV-3	6	9	Required K-walker, severe dysarthria	N/A	Axonal sensory neuropathy	Moderate to severe cerebellar hemisphere and vermian atrophy

BA = bulbar atrophy; CA = cerebellar atrophy; N/A = not available; SN = sensitive neuropathy; WM = white matter.

Variable penetrance of the condition was noted with the obligate carrier II-1 being unaffected at age 61 years and two other relatives (III-5 and III-7) at ages 37 and 33 years, respectively, manifesting neuropathies but no ataxia (Tables 1–3). Linkage analyses identified four chromosomal intervals on chr.1q24.2–q25.2, 2p21–p16.1, 10p14-p13, and 15p21.3-q23, all with a peak LOD-score = 1.66, which was the maximum LOD-score

TABLE 2. Additional Clinical Features of Affected Individuals with *PNPT1* Variations in the French Index Cases from Family 360 and Family 461, and in Carriers from the Australian Family A1

Patient	Age at Exam	Age at Onset	Ocular Signs	Reflexes (Plantar Reflex)	Vibration Sense at Ankles	Urinary Symptoms	Hearing Loss	Cognitive Impairment	Additional Signs
360–28 (index)	22	17 mo	Square waves jerks, NS hypermetric	Absent (flexor)	Abolished	None	Yes	None	Scoliosis, facial tics, vomiting, pas cavus, wasting
	32	17 mo	Square waves jerks, NS hypermetric	Absent (flexor)	Abolished	None	Yes	None	Cough
	50	17 mo	Down beat NS	Absent (unilateral extensor)	Abolished	None	Deafness	None	Cramps
461–7 (index)	40	23	NS and slow saccades	Absent (flexor)	Abolished	None	Deafness	None	None
A1-II-3	58	21	Impaired vestibulo-ocular reflex gain, NS, hypermetric saccades	Absent reflexes in upper and lower limbs, extensor plantar responses	Impaired	None	Conductive loss on right	None	Pes cavus, claw toes, diminished sensation in feet, scoliosis
A1-II-1	56	56	Mild tortional/see-saw NS, very mild upbeat NS on upgaze	Normal	N/A	N/A	N/A	N/A	Normal sensation
A1-III-1 (index)	20	10	Restriction of upper and lateral gaze, no NS	Absent reflexes and equivocal plantar responses	Reduced	N/A	N/A	N/A	Scoliosis
A1-III-2	21	20	No NS	Absent reflexes, extensor plantar responses	Reduced	N/A	No	None	Scoliosis
A1-III-5	37			Reduced reflexes	N/A	N/A	N/A	None	Nil
A1-III-7	33		No NS	N/A	N/A	N/A	N/A	None	Nil
A1-IV-1	6	5	NS	Absent reflexes	N/A	N/A	N/A	None	Scoliosis
A1-IV-2	6	5	NS	Absent reflexes	N/A	N/A	N/A	Struggles with school work	Nil
A1-IV-3	6	9	Mild NS, dysmetria, oculomotor apraxia	Absent knee jerks and reduced ankle jerks	N/A	N/A	N/A	None	Nil

N/A = not available; NS = nystagmus.

achievable in this family (Fig 1C). The chromosome 2 linkage region identified in this family falls entirely within the *SCA25* region delineated above. Combined analysis of WES and WGS and filtering of variants, which segregated with the disease within the *SCA25 locus* revealed four heterozygous substitutions in the genes encoding DNA mismatch repair protein MSH6 (*MSH6*; NM_000179.2:c.2633T>C; p.Val878Ala), stonin-1 (*STON1*; NM_001198595.1:c.1231G>A; p.Glu411Lys), proteasome activator complex subunit 4 (*PSME4*; NM_014614.2:c.3400G>A; p.Glu1134Lys), and polyribonucleotide nucleotidyltransferase PNPase 1 (*PNPT1*; NM_033109.5:c.2014-3C>G). Neither CNV nor putative pathogenic expansion within the region of linkage was detected (data not shown). Among these four candidates, *PNPT1* was the only gene in the *SCA25 locus* to be affected in both large families.

Screening of *PNPT1* in a cohort of 796 French individuals with ataxia identified a frameshift variant (NM_033109.5:c.2091delA; p.Lys697AsnfsTer6) in an individual suffering from deafness evidenced shortly after birth, and gait ataxia which began at age 23 years. The clinical presentation included dysarthria, dystonia, sensory neuropathy, nystagmus, visual impairment, and deafness (Tables 1 and 2). Segregation analysis showed that this variant was inherited from his father, who remained clinically unaffected at age 86 years. The location of these three variants within the PNPase structure is presented in Figure 2.

The functional effects of the variant from the French families was assessed in primary fibroblasts. Given the proximity of the c.2069 + 3A>G substitution with the canonical splicing donor site of exon 25, a modification of *PNPT1* transcript was predicted. A complete skipping of exon 25 affecting one strand was observed in carriers following Sanger sequencing of *PNPT1* transcript (Fig 3A). The abnormal splicing disrupts the reading frame, leading to a premature stop codon in the S1 RNA binding domain of PNPase (p.Gln672ArgfsTer18). Treatment of

TABLE 3. Motor Nerve Conduction, Sensory Nerve Action Potentials, and Electromyographic Measurements

Motor nerve conduction	360-28[a]	360-32[a]	A1-III-7	A1-IV-2	A1-IV-3	Reference Values
Median nerve						
Velocity (m/sec)	53	50	54.5	55.3	53.3	>48
Amplitude (mV)	12	3.8	11	5.2	7.3	>5
Distal latency (msec)	2.6	3.4	7	1.7	3	<3.6
Peroneal nerve						
Velocity (m/sec)	45	49.8	55.0[b]	56.0[b]	54.2	>42
Amplitude (mV)	2.4	3.2	13	13.9	2.4	>2
Distal latency (msec)	4.3	5.3	4.3	3.3	3.2	<5
Sensory nerve action potentials						
Median nerve (μV)	NR	NR	9	NR[c]	NR	>12
Sural nerve (μV)	NR	NR	7.4	NR	NR	>10
Needle electromyography	Normal	Normal	The MUAPs were large in size but with normal morphology with no increased insertional activity and normal interference pattern	Normal	Normal	

[a]From Stevanin et al.[1]
[b]Tibial nerve.
[c]Ulnar nerve.
MUAP = motor unit action potential; NR = not recordable.

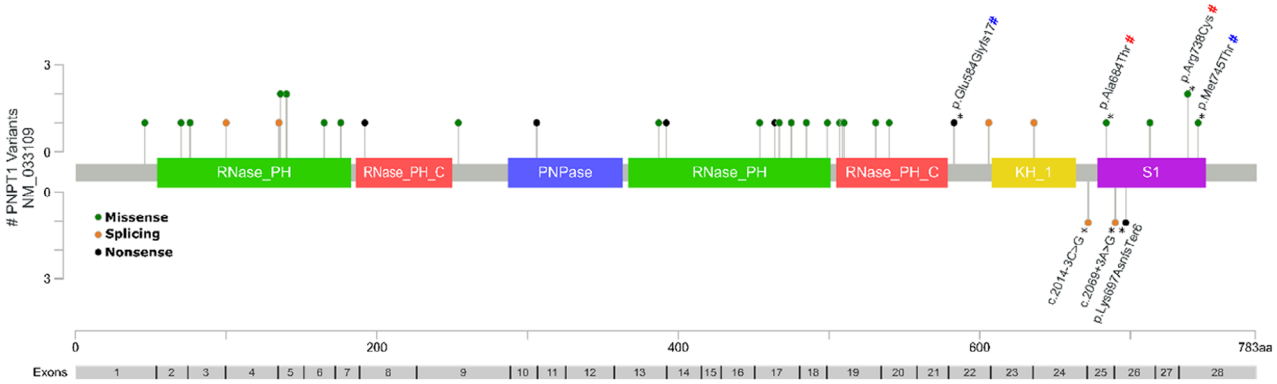

FIGURE 2: Lollipop plot and exon map depicting the distribution of pathogenic variants in the polynucleotide phosphorylase (PNPase) protein. Bi-allelic variants previously described in the literature are shown above the protein schematic. Heterozygous variants identified in this study are shown below. Variants reported in individuals with ataxia are marked by the asterisk*. All reported individuals with bi-allelic variants that present with ataxia are compound heterozygotes. Each pair of variants in an individual with ataxia is marked with a different color #. RNase_PH = 3′ exoribonuclease family, domain 1; Rnase_PH_C = 3′ exoribonuclease family, domain 2; PNPase = polyribonucleotide nucleotidyltransferase, RNA binding domain; KH_1 = KH domain; S1 = S1 RNA binding domain.

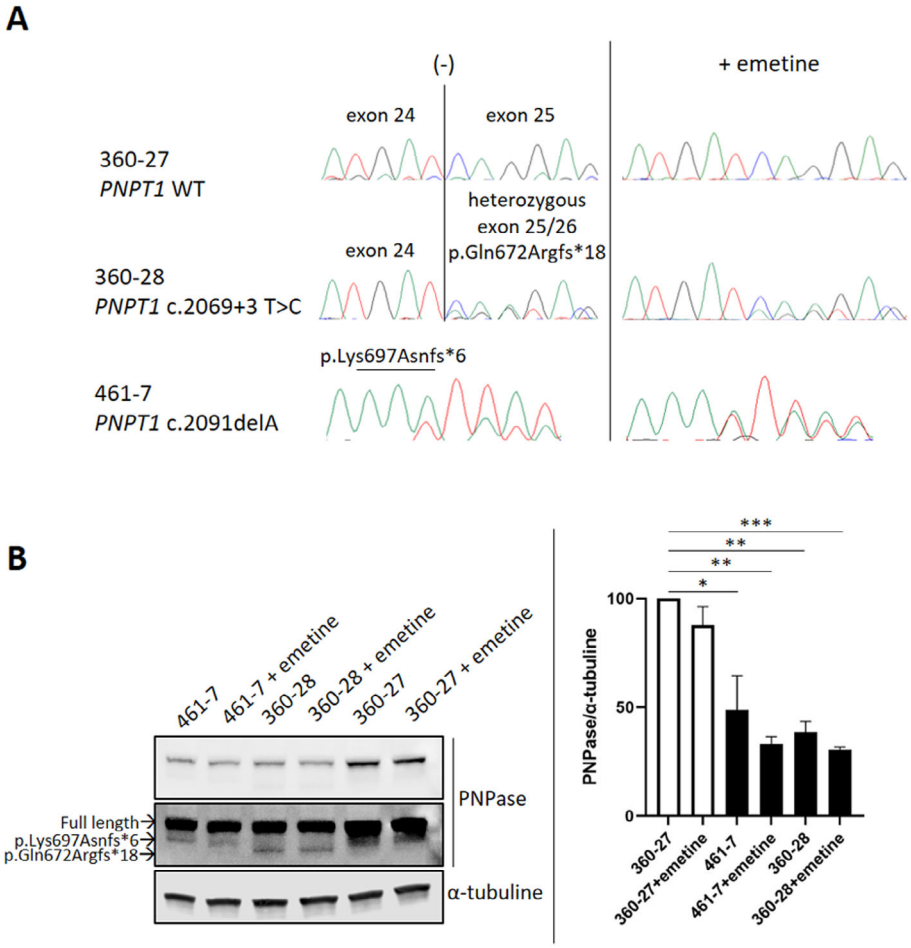

FIGURE 3: *PNPT1* variants alter transcripts and PNPase protein levels. (A) Analysis of *PNPT1* transcripts from fibroblasts cultured with or without emetine in two patients (360–28 and 461–7) *vs.* a non-carrier (360–27). Alterations of the wild-type sequence of the transcript are indicated. (B) Immunoblots of PNPase in the corresponding fibroblasts. Bands corresponding to PNPase are shown with two different time of exposure (the longer being below). Quantitation of signal intensities from two independent blots is presented on the right panel. The steadystate level of PNPase in the untreated control fibroblasts (360–27) has been adjusted to 100% and the other samples normalized to this result, showing significant reduction in affected carriers compared (black bar) to control (open bar). *$p < 0.05$, **$p < 0.01$, ***$p < 0.001$.

the cells with emetine suggested the aberrant transcript was not subject to nonsense-mediated mRNA decay (NMD). RT-PCR followed by Sanger sequencing of the p.Lys697AsnfsTer6 variant in French family 461 showed a similar escape from NMD (Fig 3A). Western blot analysis revealed that both heterozygous variants lead to a strong decrease in PNPase steady-state level (Fig 3B). Prolonged exposure of the membrane allowed the detection of additional bands with a lower molecular weight, corresponding to the predicted weight of truncated proteins encoded by mutated alleles. The negligible quantity of truncated PNPase compared to the full-length protein may reflect a post-translational degradation of abnormal proteins.

Functional effects of the variant observed in the Australian family were investigated using RNA studies of a lymphoblast line established from A1-IV-2. Splice AI predicted the loss of the normal exon 25 acceptor and the

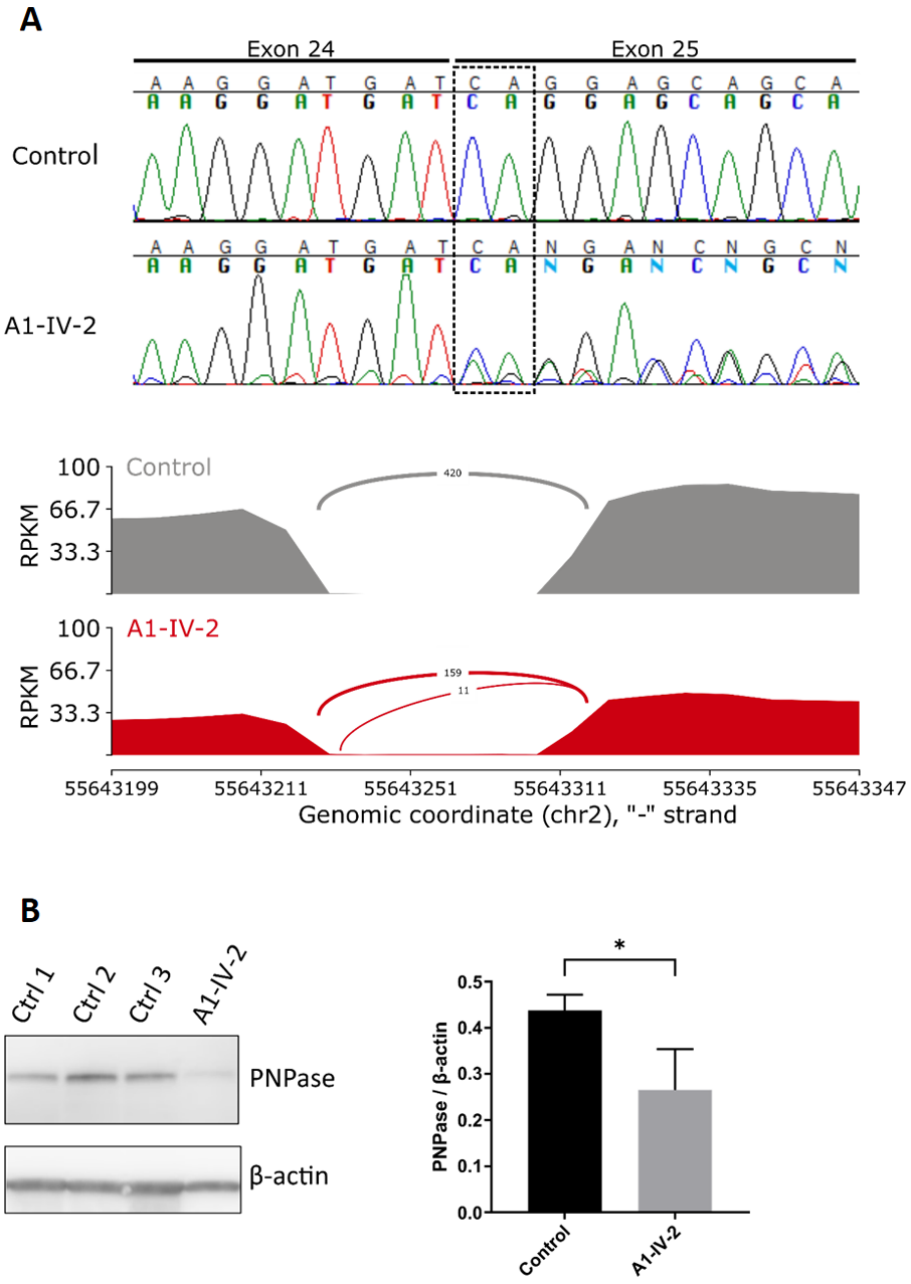

FIGURE 4: Analysis of *PNPT1* transcripts and PNPase proteins levels from lymphoblast cells from A1-IV-2. (A) Sanger sequence of RT-PCR products spanning exon 24–26 identified an aberrant transcript, which was confirmed by RNAseq analysis. The relative expression level of *PNPT1* suggested the mutant allele was being degraded by NMD. (B) Western blot analysis suggested a decrease in steadystate PNPase levels in patient-derived lymphoblasts cells and quantitation of three independent blots confirmed a significant reduction compared to control. *$p < 0.05$, **$p < 0.01$, ***$p < 0.001$.

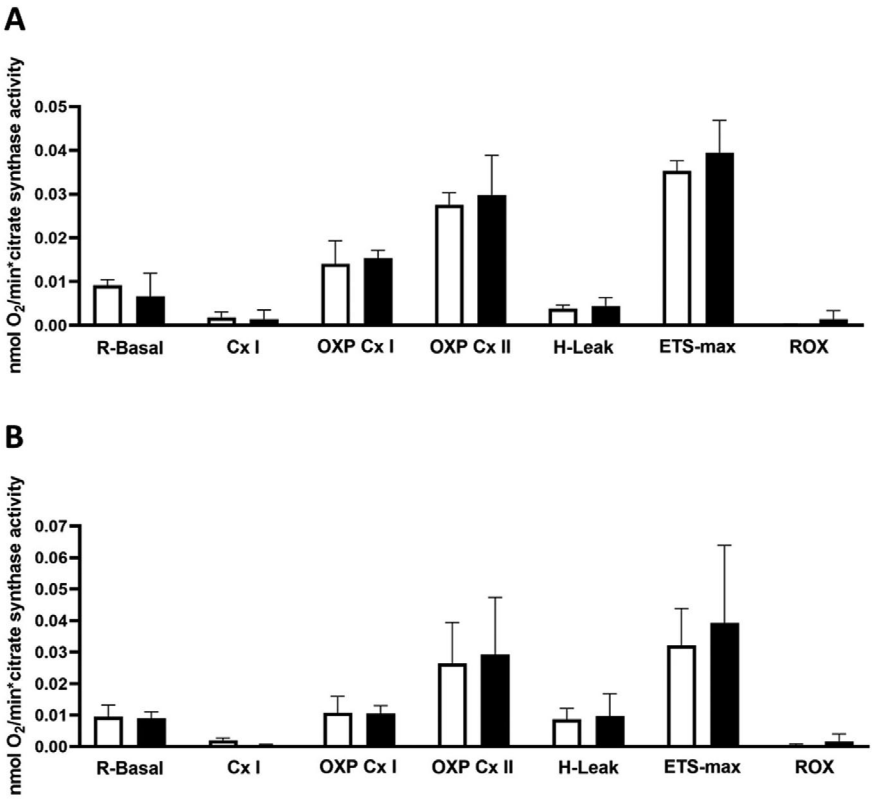

FIGURE 5: Activities of OXPHOS enzyme complexes in primary fibroblasts. Comparison of 360–27 (open bar, non-carrier) vs. (A) 360–28 (black bar, carrier) or (B) 461–27 (black bar, carrier). Cells had the same number of passages and were grown simultaneously in each comparison. Cells were then lysed to quantify protein content using the Bradford reagent. Citrate synthase (CS) activity was determined with a colorimetric assay based on the reaction between 5,5′-dithiobis-(2-nitrobenzoic acid) (DTNB) and CoA-SH to form 5-thio-2-nitrobenzoic acid (TNB). Each sample was run in duplicate and CS activity was expressed as units /min/mg of total protein. The oxygen consumption rate for each sample was finally expressed in nmol O_2/min*CS activity. Means of normalized values from two separate experiments are presented for each comparison. R-Basal: respiration under basal conditions; Cx I: complex I activity; OXP Cx I: oxidative phosphorylation involving complex I and V; OXP CxII: oxidative phosphorylation of complex I, V and II; H-Leak: measure of proton leakage; ETS-max: maximal capacity of respiration; ROX: non-mitochondrial respiration.

gain of an acceptor at nucleotide position c.2014–4/3, resulting in a predicted frameshift and premature stop codon (p.Gln672SerfsTer6). RT-PCR followed by Sanger sequencing confirmed the effect of the variant on RNA splicing (Fig 4A). Similarly, RNAseq analysis revealed that the abnormal transcript used the alternate acceptor site and accounted for approximately 10% of reads. Notably, the normalized read depth of *PNPT1* in A1-IV-2 was ~50% of the controls. Western blot analysis of lymphoblasts derived from A1-IV-2 and three controls confirmed steady-state levels of PNPase were significantly reduced in A1-IV-2 compared to the control lines (Fig 4B).

PNPT1 variants were previously associated with severe encephalomyopathy and hereditary hearing loss in bi-allelic carriers (MIM: 614934).[21,22] The mitochondrial localization of the translated protein PNPase and the association of bi-allelic variations with respiratory-chain deficiency notably lead to the linking of mutations of *PNPT1* with mitochondrial disorders and combined oxidative phosphorylation deficiency 13 (MIM: 614932).[22] Subsequently, functional assays to detect respiratory chain defects were performed, with conflicting results.[23–25] Oxidative Phosphorylation (OXPHOS) enzyme activities were measured using primary fibroblasts from the two brothers 360–27 (healthy non-carrier) and 360–28 (affected, heterozygous carrier) and from patient 461–7, also a heterozygous carrier. Mitochondrial respiration was not decreased in carriers of *PNPT1* variations compared with a non-carrier (Fig 5), suggesting that testing for OXPHOS deficiency may not be an appropriate way to investigate the cellular consequences of *PNPT1* pathogenic variants, as previously reported in bi-allelic carriers.[25]

More recently, bi-allelic pathogenic variants of *PNPT1* have been shown to trigger a type I interferon response linked to a defect in mtRNA processing.[17,25–27] Thus, we evaluated the interferon-stimulated genes (IGS) transcriptional response in PBLs from individuals with

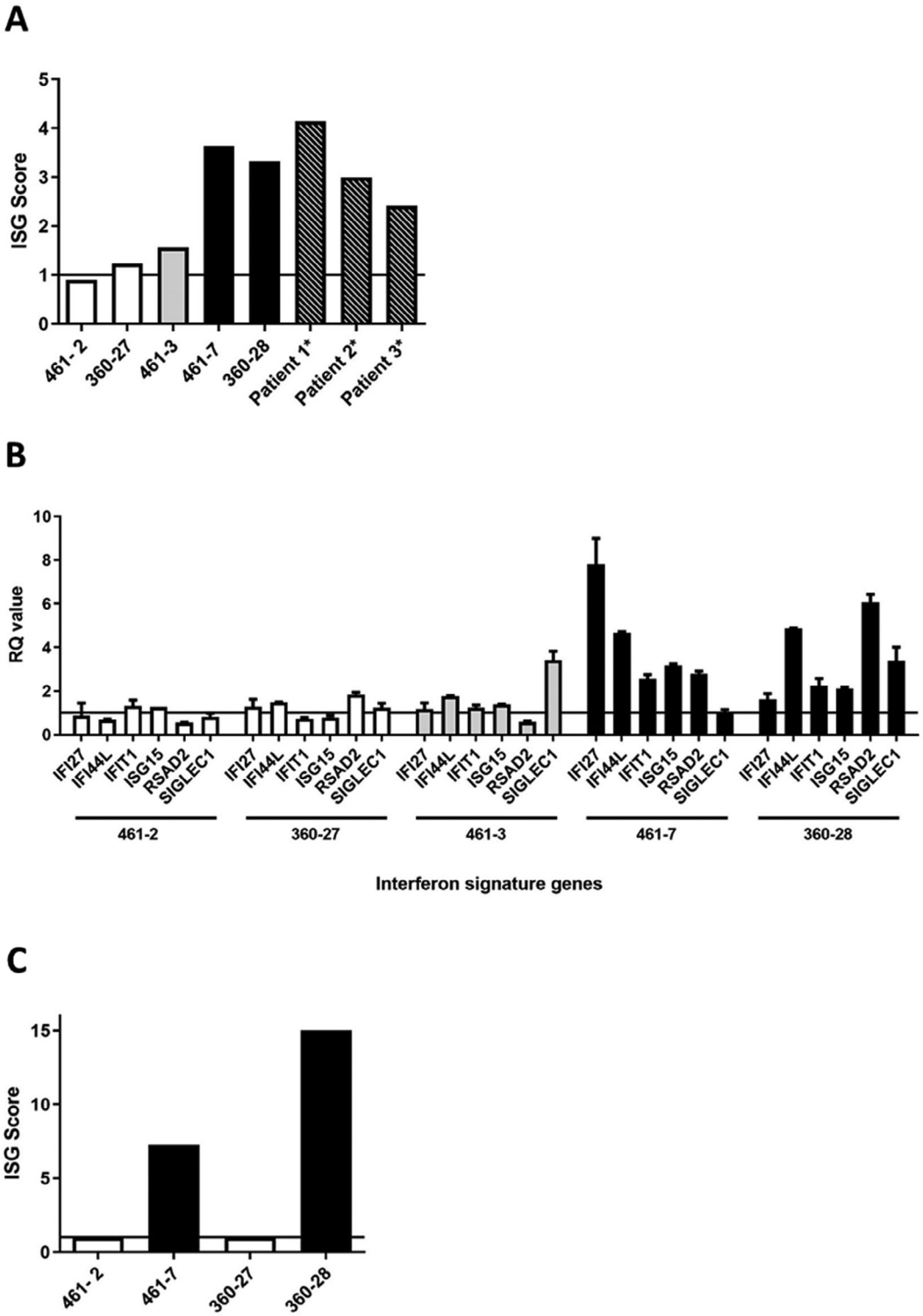

FIGURE 6: Activation of interferon-stimulated genes (ISGs) in affected individuals with heterozygous variations of *PNPT1*. (A) Aggregate ISG scores in blood: individual value of ISG score in PBLs of non-carriers (open bar), one healthy carrier (gray bar) and two patients (black bars). ISG values from three patients with homozygous variations of *PNPT1* (marked with an asterisk, striped bars) previously published by Dhir et al. have been added for comparison. (ISG score = 1, solid line) (B) RT–qPCR analysis of the six individual genes that make up the aggregate ISGs in whole blood from non-carriers (open bars) 461–2 (82 years at sampling) and 360–27 (47 years at sampling), asymptomatic carrier (gray bar) 461–3 (86 years at sampling), and patients (black bars) 461–7 (43 years at sampling) and 360–28 (46 years at sampling). The data plotted (mean and SD from duplicates) are relative quantification (RQ) values for each gene per patient. (C) Replication of aggregate ISG scores from affected carriers with blood sampled independently at different ages; 461–7 = 34 years at sampling and 360–28 = 21 years at sampling.

heterozygous variants and in controls (Fig 6A). The relative expression of six genes was used to compute an ISG score for each individual (Fig 6B), as described previously.[17] ISG scores were higher in the two unrelated individuals with *PNPT1* variants compared to non-carriers. Notably, ISG values measured in affected individuals were in the same range as those previously reported in individuals with bi-allelic pathogenic variants in *PNPT1*.[17,25,27] The ISG score for the unaffected individual carrying a pathogenic *PNPT1* variant was close to the score measured in non-carrier (control) individuals. The same difference between affected carriers and non-carriers was observed in a second experiment performed with independent PBLs collected at a different age at sampling for individuals with a pathogenic variant (Fig 6C).

Discussion

The genetic basis of the *SCA25 locus* had eluded discovery since the disorder was first mapped in 2004. In this study, we identified nonsense splice variants in *PNPT1* in two large families with autosomal dominant spinocerebellar ataxia that map to the *SCA25 locus*. Analysis of *PNPT1* in a cohort of 796 individuals with SCA led to the detection of one additional individual with a nonsense variant. Bi-allelic pathogenic variants in *PNPT1* have been previously associated with variable diseases ranging from non-syndromic hearing loss to multisystem Leigh disease, and with other clinical conditions including visual defects, abnormal muscle tone, speech delays, feeding difficulties, scoliosis, and/or sensory neuropathy.[21,22,24–26,28–30] These previously described clinical conditions were all observed in families with a recessive model of inheritance. Many of these symptoms are overlapping with the clinical presentation of the individuals we have identified with heterozygous *PNPT1* variants. However, the majority of symptoms described in individuals with bi-allelic pathogenic variants appeared in the first year of life, in contrast to those with a heterozygous variant, in whom symptoms appeared at ages ranging from first months of life through to incomplete penetrance at age 86 years for the oldest healthy carrier.[1,25,27] This indicates that penetrance may be lower, and expressivity more variable in individuals with heterozygous variants. In the previous studies describing bi-allelic variants in *PNPT1*, very little information was reported regarding the heterozygous parents, suggesting that they were healthy at the time of publication. An alternative explanation for the apparent lack of clinical presentation in heterozygous carriers of pathogenic bi-allelic variants could be the location of the variants, resulting in a possible genotype–phenotype correlation for the risk of developing ataxia. The three variants described in our study are all located in the S1-domain (Fig 2). Strikingly, two of them alter the protein sequence from the same amino-acid position, and all induce a premature stop in the S1-domain. In contrast, previous studies demonstrate pathogenic bi-allelic variants, indicated above the protein schematic, are located throughout the gene. Only two previous reports described patients with bi-allelic *PNPT1* variants who developed ataxia in adulthood. All of these patients had missense variants within the S1-domain, leading the authors to hypothesize a genotype-correlation.[25,30] Thus, it is reasonable to speculate that variants affecting the S1 domain, which has a crucial role in RNA binding, may be associated with ataxia.

PNPase is localized to the mitochondrial matrix and the intermembrane space.[21,22,29] Dysfunction of mitochondria has been described in Friedreich's ataxia and SCA28. Similarly, defective mitochondrial mRNA maturation was described in recessive spastic ataxia due to mutations in *MTPAP*.[31] Among all of the SCA loci, *PNPT1* is the first gene linked with the sensing and elimination of double-stranded mtRNA, reinforcing the role of mtRNA processing in inherited ataxias and more broadly in neurodegenerative disorders. Indeed this exoribonuclease is reported to play a dual role in RNA import into the mitochondria, and in preventing the accumulation of double-stranded mtRNA in mitochondria.[17,21,22,29] Variants affecting the S1-domain, which reduce the expression of PNPase and/or which lead to proteins lacking this domain, may alter or destabilize the homotrimeric structure of the enzyme. This mechanism, through a dominant-negative effect, might be the basis of the genotype–phenotype correlation. Alternatively, variants affecting the S1-domain could lead to altered enzyme function. A previous study showed that two disease-linked missense variants located before the S1-domain caused dimer formations, while truncated PNPase lacking the S1-domain formed trimer, with different altered function.[32] Therefore, it is possible that mutations removing or altering the S1-domain (as observed in patients who developed ataxia) lead to different PNPase enzymatic structures compared to missense variants located upstream the S1-domain. Altered sensing of certain mtRNA may be the molecular basis of the apparent correlation between ataxia and variants affecting the S1-domain. Such correlations often highlight specific mechanisms that partly explain the clinical variability among carriers of pathogenic variants in the same gene in mendelian disorders. Analysis of the GTEx database (https://gtexportal.org/home/; V8) suggests that *PNPT1* expression is elevated in cerebellar tissues compared to other brain regions and that there is a distinct signature of *PNPT1* isoform expression in cerebellum. Collectively, the specific effect of variants located in the S1-domain on the enzymatic structure and the expression pattern of *PNPT1* in cerebellar tissues may explain the correlation of mutations affecting the S1-domain with ataxia.

Individuals with bi-allelic variants in *PNPT1* display mitochondrial double-stranded RNA accumulation with a subsequent leakage into the cytosol, leading to aberrant type I interferon activation.[17] In our series, the ISG scores were higher in affected heterozygous carriers compared with non-carriers, suggesting that the same triggering of a type I interferon response occurs in individuals with both bi-allelic and heterozygous variants in this gene. This aberrant response may also contribute to the development of disease. An increased IFN activation may drive neuroinflammation leading to neuronal dysfunction and/or neuronal loss. For example, it has been proposed that the chronic production of interferon-α (IFNα) from astrocytes drives the neurodegeneration and the appearance of ataxia in a mouse model of Aicardi-Goutières syndrome (AGS), a well-known interferonopathy.[33,34] However, a functional link between PNPase mediated type I interferon response and neuropathology is yet to be tested in individuals with either heterozygous or bi-allelic *PNPT1* variants. Our study cannot definitively determine if this activation is involved in the pathogenesis, or alternatively is merely a biological marker of the disease. Interestingly, the ISG score in the heterozygous carrier still healthy at age 86 was close to the values measured in non-carriers. This result suggests the limitation of the type I interferon response may directly or indirectly prevent deleterious effects of pathogenic *PNPT1* variations. The identification of an aberrant type I interferon response in other interferonopathies led to therapeutic trials targeting this pathway. The use of Janus kinase (JAK) 1 inhibitor in AGS has showed promising but also variable results.[35–37] JAK 1/2 are part of the type I interferon-receptor complex that could be targeted in *PNPT1* carriers, although reversing the neurodegeneration in affected individuals with a very early onset may be challenging.[38]

A variable type I interferon response among carriers may also explain the striking intrafamilial variability observed in SCA25. Variable penetrance is a widespread phenomenon in mendelian disorders, especially in dominant diseases, and to date poorly understood. We searched for modifiers variants in ten genes belonging to the cGAS-STING pathway, associated with the type I interferon response (*STING, IFI44, IFI44L, IFIT1, SIGLEC1, IFI27, ISG15, RSAD2, IFI6, OTOF*) but did not detect potential modifying variants shared by our patients (data not shown). We also looked in other genes directly involved in the sensing of double-stranded mtRNAs (*SUPV3L1* and *MDA5*), without significant findings. Similarly, intermediate alleles of some expanded repeat loci have been reported to be risk factors for other neurodegenerative disorders.[39,40] However, all of the expansion loci examined in our patients (n = 30) encoded repeat in the normal range. Thus, the genetic basis of the variable penetrance in SCA25 remains to be elucidated.

To conclude, our work not only describes *PNPT1* as causing SCA25, but also establishes a link between SCA25 and Mendelian type I interferonopathies, highlighting a common pathological pathway and possibly the hope of common treatments. How the alteration of mtRNA trafficking and the subsequent aberrant type I interferon response caused by *PNPT1* variants affecting the PNPase S1-domain might then lead to cerebellar dysfunction remains to be explained.

Acknowledgments

Part of this work was carried out on the iGenSeq sequencing and the Data Analysis Core bioinformatic facilities of the ICM. The authors would like to thank Michael Wilson, Greta Gillies, and Kate Pope (Murdoch Children's Research Institute) for their technical assistance. We thank the patients and their families for participation in this study.

The research leading to these results has received funding from the program "Investissements d'avenir" ANR-10- IAIHU-06 and ANR-11- INBS-0011—NeurATRIS: Translational Research Infrastructure for Biotherapies in Neurosciences. European funding: 6th PCRD (EUROSCA, to A.B.), 7th PCRD (Neuromics, to A.B.) et H2020 (SOLVE-RD, to G.S.); Agence Nationale de la Recherche (ANR SPATAX-QUEST, to G.S.), Association Connaitre les Syndromes Cérébelleux (to G.S.) and Fondation Maladies Rares (to G.S.).

This work was supported in part by NHMRC GNT2001513 to PJL and MBD. Additional funding was provided by the Independent Research Institute Infrastructure Support Scheme and the Victorian State Government Operational Infrastructure Program. Whole Genome Sequencing for the Australian family was funded through the Austin Health Adult Undiagnosed Diseases Program, which is supported by Austin Health and the Victorian Medical Research Acceleration Fund.

Me.B. was supported by an Australian National Health and Medical Research Council (NHMRC) Senior Research Fellowship (1102971). K.C.D. was supported by an Australian Research Training Program Scholarship. R.M.T. was supported by an Australian Postgraduate Award and funding from the Edith Moffat fund. K.B.H. was suppported by an NHMRC Early Career Fellowship, and a Melbourne Children's Clinician Scientist Fellowship. B.R.E.A. was supported by an NHMRC Early Career Fellowship (1157776). P.J.L. was funded by the Vincent Chiodo Foundation.

Italian Ministry for Education, University and Research (Ministero dell'Istruzione, dell'Università e della Ricerca—MIUR) under the programme "Dipartimenti di Eccellenza 2018–2022" Project code D15D18000410001 to Alfredo Brusco.

H.R. was supported by an NHMRC EL1 Investigator Grant (1194364).

Author Contributions

Ma.B., Me.B., O.C., A.R., A.B., M.B.D., G.S., P.J.L., and A.D. contributed to the conception and design of the study. Ma.B., Me.B., A.P., M.J., R.M.T., C.E., K.C.D., P.L.-C., C.C., H.R., N.A., B.R.E.A., Ivd.S., K.B.H., M.C., D.J.A., E.M., L.G.-N., E.S., R.J.McK.G., M.J.W., A.B., R.J.L., M.B.D., G.S., P.J.L., and A.D. contributed to the acquisition and analysis of data. Ma.B., Me.B., M.B.D., K.C.D., P.J.L., and A.D. contributed to drafting the text or preparing the figures.

Potential Conflicts of Interests

The authors declare no competing interests.

References

1. Stevanin G, Bouslam N, Thobois S, et al. Spinocerebellar ataxia with sensory neuropathy (SCA25) maps to chromosome 2p. Ann Neurol 2004;55:97–104.
2. 1,000 Genomes Project Consortium, Abecasis GR, Auton A, et al. An integrated map of genetic variation from 1,092 human genomes. Nature 2012;491:56–65.
3. Henden L, Wakeham D, Bahlo M. XIBD: software for inferring pairwise identity by descent on the X chromosome. Bioinformatics 2016;32:2389–2391.
4. Leutenegger A-L, Prum B, Génin E, et al. Estimation of the inbreeding coefficient through use of genomic data. Am J Hum Genet 2003; 73:516–523.
5. Bahlo M, Bromhead CJ. Generating linkage mapping files from Affymetrix SNP chip data. Bioinformatics 2009;25:1961–1962.
6. Lessel D, Vaz B, Halder S, et al. Mutations in SPRTN cause early onset hepatocellular carcinoma, genomic instability and progeroid features. Nat Genet 2014;46:1239–1244.
7. Wang K, Li M, Hadley D, et al. PennCNV: an integrated hidden Markov model designed for high-resolution copy number variation detection in whole-genome SNP genotyping data. Genome Res 2007;17:1665–1674.
8. Dolzhenko E, Deshpande V, Schlesinger F, et al. ExpansionHunter: a sequence-graph-based tool to analyze variation in short tandem repeat regions. Bioinformatics 2019;35:4754–4756.
9. Dolzhenko E, Bennett MF, Richmond PA, et al. ExpansionHunter Denovo: a computational method for locating known and novel repeat expansions in short-read sequencing data. Genome Biol 2020;21:102.
10. Tankard RM, Bennett MF, Degorski P, et al. Detecting expansions of tandem repeats in cohorts sequenced with short-read sequencing data. Am J Hum Genet 2018;103:858–873.
11. Dobin A, Davis CA, Schlesinger F, et al. STAR: ultrafast universal RNA-seq aligner. Bioinformatics 2013;29:15–21.
12. Li H, Handsaker B, Wysoker A, et al. The sequence alignment/map format and SAMtools. Bioinformatics 2009;25:2078–2079.
13. Liao Y, Smyth GK, Shi W. featureCounts: an efficient general purpose program for assigning sequence reads to genomic features. Bioinformatics 2014;30:923–930.
14. Law CW, Alhamdoosh M, Su S, et al. RNA-seq analysis is easy as 1–2-3 with limma, Glimma and edgeR. F1000Res 2016;5:ISCB Comm J-1408.
15. Stephenson SEM, Aumann TD, Taylor JM, et al. Generation and characterisation of a parkin-Pacrg knockout mouse line and a Pacrg knockout mouse line. Sci Rep 2018;8:7528.
16. Jeremiah N, Neven B, Gentili M, et al. Inherited STING-activating mutation underlies a familial inflammatory syndrome with lupus-like manifestations. J Clin Invest 2014;124:5516–5520.
17. Dhir A, Dhir S, Borowski LS, et al. Mitochondrial double-stranded RNA triggers antiviral signalling in humans. Nature 2018;560: 238–242.
18. Cortese A, Simone R, Sullivan R, et al. Biallelic expansion of an intronic repeat in RFC1 is a common cause of late-onset ataxia. Nat Genet 2019;51:649–658.
19. Rafehi H, Szmulewicz DJ, Bennett MF, et al. Bioinformatics-based identification of expanded repeats: a non-reference intronic pentamer expansion in RFC1 causes CANVAS. Am J Hum Genet 2019; 105:151–165.
20. Kircher M, Witten DM, Jain P, et al. A general framework for estimating the relative pathogenicity of human genetic variants. Nat Genet 2014;46:310–315.
21. von Ameln S, Wang G, Boulouiz R, et al. A mutation in PNPT1, encoding mitochondrial-RNA-import protein PNPase, causes hereditary hearing loss. Am J Hum Genet 2012;91:919–927.
22. Vedrenne V, Gowher A, De Lonlay P, et al. Mutation in PNPT1, which encodes a polyribonucleotide nucleotidyltransferase, impairs RNA import into mitochondria and causes respiratory-chain deficiency. Am J Hum Genet 2012;91:912–918.
23. Matilainen S, Carroll CJ, Richter U, et al. Defective mitochondrial RNA processing due to PNPT1 variants causes Leigh syndrome. Hum Mol Genet 2017;26:3352–3361.
24. Alodaib A, Sobreira N, Gold WA, et al. Whole-exome sequencing identifies novel variants in PNPT1 causing oxidative phosphorylation defects and severe multisystem disease. Eur J Hum Genet 2016;25: 79–84.
25. Rius R, Van Bergen NJ, Compton AG, et al. Clinical spectrum and functional consequences associated with bi-allelic pathogenic PNPT1 variants. J Clin Med 2019;8(11). doi:10.3390/jcm8112020
26. Bamborschke D, Kreutzer M, Koy A, et al. PNPT1 mutations may cause Aicardi-Goutières-Syndrome. Brain and Development 2021; 43:320–324.
27. Pennisi A, Rötig A, Roux C-J, et al. Heterogeneity of PNPT1 neuroimaging: mitochondriopathy, interferonopathy or both? J Med Genet 2022;59:204-208.
28. Slavotinek AM, Garcia ST, Chandratillake G, et al. Exome sequencing in 32 patients with anophthalmia/microphthalmia and developmental eye defects. Clin Genet 2015;88:468–473.
29. Sato R, Arai-Ichinoi N, Kikuchi A, et al. Novel biallelic mutations in the PNPT1 gene encoding a mitochondrial-RNA-import protein PNPase cause delayed myelination. Clin Genet 2018;93:242–247.
30. Eaton A, Bernier FP, Goedhart C, et al. Is PNPT1-related hearing loss ever non-syndromic? Whole exome sequencing of adult siblings expands the natural history of PNPT1-related disorders. Am J Med Genet A 2018;176:2487–2493.
31. Crosby AH, Patel H, Chioza BA, et al. Defective mitochondrial mRNA maturation is associated with spastic ataxia. Am J Hum Genet 2010; 87:655–660.

32. Golzarroshan B, Lin C-L, Li C-L, et al. Crystal structure of dimeric human PNPase reveals why disease-linked mutants suffer from low RNA import and degradation activities. Nucleic Acids Res 2018;46: 8630–8640.

33. Akwa Y, Hassett DE, Eloranta ML, et al. Transgenic expression of IFN-alpha in the central nervous system of mice protects against lethal neurotropic viral infection but induces inflammation and neurodegeneration. J Immunol 1998;161:5016–5026.

34. Campbell IL, Krucker T, Steffensen S, et al. Structural and functional neuropathology in transgenic mice with CNS expression of IFN-alpha. Brain Res 1999;835:46–61.

35. Crow YJ, Stetson DB. The type I interferonopathies: 10 years on. Nat Rev Immunol 2021;1-13.

36. Neven B, Al Adba B, Hully M, et al. JAK inhibition in the aicardi-goutières syndrome. N Engl J Med 2020;383:2190–2191.

37. Vanderver A, Adang L, Gavazzi F, et al. Janus kinase inhibition in the aicardi-goutières syndrome. N Engl J Med 2020;383: 986–989.

38. Crow YJ, Shetty J, Livingston JH. Treatments in Aicardi-Goutières syndrome. Dev Med Child Neurol 2020;62: 42–47.

39. Elden AC, Kim H-J, Hart MP, et al. Ataxin-2 intermediate-length polyglutamine expansions are associated with increased risk for ALS. Nature 2010;466:1069–1075.

40. Lattante S, Millecamps S, Stevanin G, et al. Contribution of ATXN2 intermediary polyQ expansions in a spectrum of neurodegenerative disorders. Neurology 2014;83:990–995.